

Elie Shammass

Assistant Professor
Department of Mechanical Engineering,
American University of Beirut,
Beirut 11-0236, Lebanon
e-mail: es34@aub.edu.lb

Daniel Asmar

Assistant Professor
Department of Mechanical Engineering,
American University of Beirut,
Beirut 11-0236, Lebanon
e-mail: da20@aub.edu.lb

Motion Planning for an Underactuated Planar Robot in a Viscous Environment

In this paper, we solve the motion planning problem for a class of underactuated multibodied planar mechanical systems. These systems interact with the environment via viscous frictional forces. The motion planning problem is solved by specifying the location of friction pads on the robot as well as by specifying the input of the actuated degrees of freedom. Moreover, through the proposed novel motion planning analysis, we identify the simplest planar swimming robot, the two-link swimmer. [DOI: 10.1115/1.4029509]

1 Introduction

Animal-inspired robots have greatly evolved over the past years. From walking to crawling to undulating, researchers adopt biometric approaches to enable robots to locomote like their biological counterparts. Yet animal locomotion remains superior in terms of energy consumption and maneuverability and researchers have been trying to close this performance gap. The ability of some animals to locomote in different media and terrains has inspired robotists to investigate locomotion in different environments. For example, biological snakes have mastered nearly every environment one can think of: they can undulate on rough terrains, swim in aquatic environments, and even glide through the air. As a result, there has been a growing interest recently in modeling robot locomotion in fluid mediums. In particular, the high maneuverability observed in fish, anguilliform, and eels has motivated researchers to design multilink (i.e., articulated) robotic swimmers, in the hope of demonstrating comparable performances.

1.1 Prior Work. The work presented in this paper has its roots in the literature related to the motion planning of underactuated robotic systems. The poster-child research problem for motion planning is parking a car with N -trailers [1,2]. This problem was addressed from several fronts: motion planning, path planning, and controllability, [3–6]. For a comprehensive historical as well as a technical exposition of the related work, the reader could consult the following Refs. [7–11]. In this paper, we address the motion planning problem of a symmetric two-link planar robot that interacts via frictional forces with its environment rather than momenta and nonholonomic constraints.

The system on which we are planning to implement our proposed motion planning method is a close relative to a system labeled as the *roller racer*. The main difference is the fact that the roller racer interacts with the environment through nonholonomic constraints rather than viscous friction. The nonholonomic motion planning problem for the roller racer was investigated by Refs. [12–14]. Whereas the roller racer is a driftless mechanical system, a key ingredient for our proposed motion planning is the existence of drift in the dynamics of the system [15–17]. In fact, drift induces a major component of motion for robotic systems that are moving within a fluid.

Mason and Burdick [18] were among the first to analyze the mechanics of deformable bodies in ideal fluids. Along the same footsteps, Kanso et al. [19] modeled the dynamics of an articulated body submerged in an ideal fluid to obtain the reconstruction equations, which describe the net locomotion of the system in terms of its shape changes. The work was extended in Ref. [20] to find the optimal shape changes that produce a desired net

locomotion, where the motion planning problem was formulated as a nonlinear optimization problem. Similarly, using the curvature of the mechanical connection from the geometric mechanics framework, Melli et al. [21] developed open-loop gaits for an articulated body with two shape variables and a simple method for trajectory tracking in the plane was devised. Nonetheless, all these works are concerned with ideal fluids or, in other words, are swimming in potential flows where no external forces are experienced. These are idealized conditions that do not include all the characteristics of flows that are encountered in the real world.

A more physical and realistic approach was developed in Ref. [22], where McIsaac and Ostrowski modeled the motion of an underwater eel robot using two different friction models: viscous and fluid drag. The fluid drag model corresponds to swimming in an inviscid fluid (at a high Reynolds number), whereas the viscous model can correspond to either gliding over dry land or swimming in a fluid where viscous effects are significant at relatively low Reynolds number. McIsaac and Ostrowski explored several types of locomotive gaits; nonetheless, there are several remarks concerning their viscous friction model. First of all, the authors neglected the frictional forces parallel to the body, whereas in this paper, the presence of such forces is crucial in generating locomotion along directions that are otherwise unreachable. Moreover, the authors assumed that the frictional forces always act at the center of a given link; however, inspired by the mechanics of friction interaction in animal locomotion, in this paper, we allow the point of contact along a link to vary by using displaceable friction pads on each link. Finally, although McIsaac and Ostrowski investigated a number of gaits, they were merely a means for validating the models by comparing the simulations to the experimental results. The general motion planning problem was not addressed and it remains unclear what shape changes are required to achieve a prescribed desired trajectory. This question is answered in the work presented in this paper.

Chernous'ko [23–26] demonstrated the motion of two-link mechanisms on a plane, assuming dry friction conditions. He presented a scheme in which any planar motion can be achieved by a combination of slow and fast motions; however, the analysis is limited to static friction scenarios. Furthermore, the success of the slow motion phase is constrained by a condition on the relative size of the two links—a condition that would be violated if the links were of equal size. Figurina [27] also studied the motion of a two-link mechanism on a plane and showed that for systems using only slow motions no prescribed positions can be attained. Again the study is limited to dry friction type scenarios.

Burton et al. [28] found a way around the Scallop theorem by introducing a buoyant moment (i.e., an offset between buoyancy point and center of mass). This gives the system a preferred orientation that breaks the reversibility constraint, thereby allowing the platform to move. Since their solution relies on the buoyant moment it cannot be applied to the motion of a symmetric two-dimensional linkage as is being considered in this paper.

Manuscript received May 29, 2013; final manuscript received December 27, 2014; published online April 2, 2015. Assoc. Editor: Jozsef Kovacsics.

Melli and Rowley [29] borrowed tools from geometric mechanics to develop a gait design technique for swimmers in potential flow and Stokes flow. As mentioned earlier, a potential flow is inconceivable in the physical world. On the other hand, a Stokes flow is one where the Reynolds number is so low that the inertial forces are neglected; a scenario that has no applications in the robotics industry. Even though, toward the end of their paper, the authors did extend the potential flow to account for viscous effects, they clearly stated that in the case of planar motion, their large-amplitude gait design technique only applies for turning gaits and not forward or lateral gaits. This motivated us to explore the motion planning problem for a planar swimmer. In fact, in our previous paper [30], we found a way around this limitation by designing an appropriate mixture of active and gliding strokes and by placing the friction pads at determined locations.

1.2 Contributions. The contributions of the paper are three-fold. First, we formally define a family of underactuated planar mechanical (UPM) systems. Then, we prove that for this family of systems, the equations of motion can be expressed in a simplified form that is adequate for the motion planning analysis problem. Lastly, coupling the simplified form of the equations with a specifically designed family of allowable inputs, the motion planning problem is solved in a novel approach, that is, by simple analysis of the equations of motion gaits are designed to locomote a system along a desired direction. An important finding of the paper is the fact that the simplest planar swimmer can be comprised of only two links. In fact, this system can locomote in the plane independently along two perpendicular directions provided that one designs the right input, or gait, and also specifies the location of the friction pads along the system's links; however, the system cannot change its orientation.

The paper is organized as follows: in Sec. 2, we formally define the under-actuated planar mechanical systems, work out the dynamic equations governing their motion, and simplify the equations of motion in preparation for the motion planning analysis problem. In Sec. 3, we address the motion planning analysis problem by first introducing an allowable set of inputs and analyzing the expected motion due to these inputs. In Sec. 4, we work out an example through which we first evaluate the reduced form of the equations of motion, then through the analysis of motion planning problem, we solve for two gaits that locomote the system along two desired directions. Finally, we conclude the paper and present the directions of our future work in Sec. 5.

2 Equations of Motion

In this section, we develop the equations of motion for UPM systems, similar to the system depicted in Fig. 1, then we "simplify" these equation in order to be ultimately utilized in solving the motion planning problem.

For the mechanical systems considered in this paper, we assume that the configuration space has a *principal fiber-bundle* structure such that $Q = G \times R$, where G is the fiber space and R is the base space. Note that, the fiber space represents the position and orientation of the system and is sometimes referred to as the operational space whereas the base space represents the shape of the system. Accordingly, a configuration variable $q \in Q$ is composed of a fiber variables and base variables such that $q = (g, r)$, where $g \in G$ and $r \in R$. Finally, let n , l , and m be the dimension of Q , G , and R , respectively, where we have $n = l + m$.

2.1 UPM Systems. The systems we are analyzing in this paper are underactuated since only the interlink angles are controlled. The other configuration variables such as position and orientation of the system, which are measured with respect to a fixed inertial frame, are not actuated.

DEFINITION 1. A mechanical system with n generalized coordinates $q \in Q$ is an underactuated mechanical system if it is subject

to a generalized actuation forces, τ_i , such that for $0 < l < n$, $\tau_i = 0$ for $i \in \{1, 2, \dots, l\}$ and $\tau_i = \tau_i(t)$ for $i \in \{l+1, l+2, \dots, n\}$.

Moreover, since we will limit the analysis to *planar* mechanical systems, the underactuation can be defined through the structure of the configuration space. Generally, the base variables, r_i , are controlled and represent the interlink variables that define the shape of the robot while the fiber variables are not controlled and represent the position and orientation of the robot.

DEFINITION 2. A mechanical system is an UPM system if it is underactuated according to Definition 1 and its configuration space has a principal fiber-bundle structure such that, $q \in Q = G \times M$, where the unactuated fiber space is $G = SE(2)$, the special Euclidean group, and the actuated base space is $R = \mathbb{S} \times \mathbb{S} \times \dots \times \mathbb{S}$, a product of rotation groups representing the actuated interlink revolute joints.

Note that since the fiber space is given by $G = SE(2)$, the special Euclidean group, an element in the fiber space is a three-dimensional vector, $g = (x, y, \theta)^T$. Next, we lay down the ground work to determine the equations of motion as well as highlight their structure, which will be exploited in solving the motion planning problem.

2.2 Configuration Variables. Let n_L be the number of uniform links in the UPM system. Each link has a mass M_i , an inertia J_i about its center of mass, and a length $2L_i$. Also, each link interacts with the environment through a friction pad that is located along the length of the link at a distance d_i from the link's center of mass as shown in Fig. 1. Hence, all contact forces between the mechanical system and the environment emanate from the friction pads.

To simplify the analysis, the dynamics of such systems is usually expressed in terms of a body-attached coordinate frame. In this paper, we utilize the following body-frame specifications. As shown in Fig. 1, we attach the origin of the body-frame to the center of mass of the *entire* system and define θ as the average of all the absolute angles α_i . The orientation of the body-attached coordinate frame and the interlink angles can be determined as

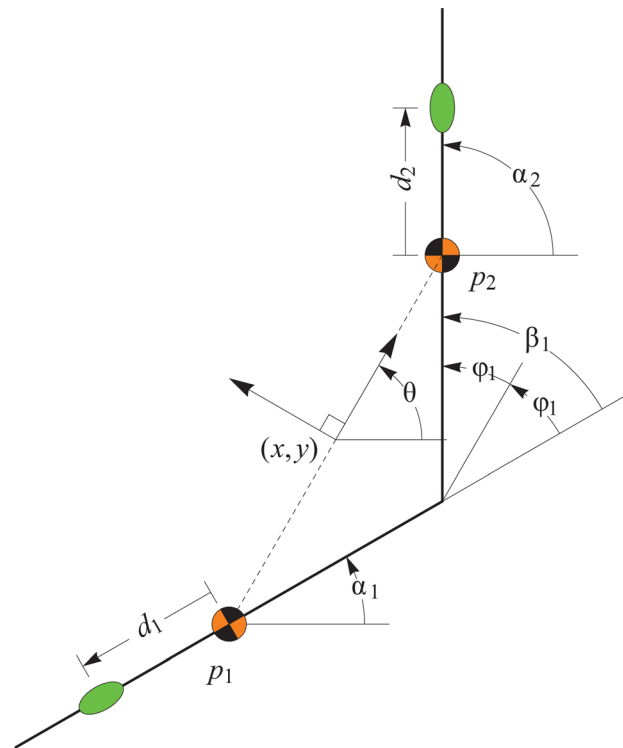


Fig. 1 A two-link underactuated planar system

$$\theta = \frac{1}{n_L} \sum_{i=1}^{n_L} \alpha_i, \text{ and } \phi_i = \frac{\beta_i}{n_L} = \frac{\alpha_{i+1} - \alpha_i}{n_L} \quad (1)$$

for $i = 1, 2, \dots, n_L - 1$. Note that the interlink angle, β_i , is a multiple of the angle, ϕ_i . This relation provides another minor simplification in the expressions of the equations of motion. Hence, the generalized coordinates, which will be used to evaluate the equations of motion, are represented in the variable

$$q = (x, y, \theta, \phi_1, \dots, \phi_{n_L-1})^T \quad (2)$$

2.3 Generalized Forces. For the UPM systems that we are considering in this paper, there are two kinds of forces that have to be accounted for: frictional and actuation forces. The interaction between the mechanical system and the environment is *viscous*, that is, the frictional dissipative force is proportional to the velocity of the friction pad. In other words, the induced frictional force is given by $f = -\mu v$, where μ is the viscous friction coefficient and v is the planar velocity of the friction pad.

Moreover, we shall assume that the viscous friction interaction between the friction pads and the environment is *anisotropic*. That is, the viscous frictional constant depends on the direction of motion with respect to the link. Accordingly, the frictional forces are given by $f_i^{\parallel} = -\mu_i v_i^{\parallel}$, and $f_i^{\perp} = -\nu_i v_i^{\perp}$, where μ_i and ν_i are, respectively, the viscous coefficients of friction for the velocities *along* i th link, v_i^{\parallel} , and for velocities *perpendicular* to the i th link, v_i^{\perp} . For UPM systems, these velocities can be determined by projecting the inertial velocities of the friction pads along the link direction and along a direction perpendicular to the link. Thus, we have

$$v_i^{\parallel} = (\cos \alpha_i \sin \alpha_i)^T \frac{d}{dt} (p_i + d_i (\cos \alpha_i \sin \alpha_i)^T) \quad (3)$$

$$v_i^{\perp} = (-\sin \alpha_i \cos \alpha_i)^T \frac{d}{dt} (p_i + d_i (\cos \alpha_i \sin \alpha_i)^T) \quad (4)$$

where p_i is the location of the i th link center of mass with respect to the fixed inertial frame. To determine the frictional forces in the equations of motion, we use the following dissipative Rayleigh power function:

$$\mathcal{P}(q, \dot{q}) = \frac{1}{2} \sum_{i=1}^{n_L} \left(\mu_i (v_i^{\parallel})^2 + \nu_i (v_i^{\perp})^2 \right) = \frac{1}{2} \dot{q}^T \mathcal{D}(q) \dot{q} \quad (5)$$

where \dot{q} is the time derivative of the generalized coordinate, q . The Rayleigh power function $\mathcal{P}(q, \dot{q})$ and its associated matrix $\mathcal{D}(q)$ simplify the evaluation of the frictional force acting on each of the generalized coordinates. In fact, for each generalized coordinate in Eq. (2) the frictional forces acting on it is given by $f_{q_i} = -\partial \mathcal{P}(q, \dot{q}) / \partial \dot{q}_i$.

The other kind of forces that could act on UPM systems are the actuation forces of the controlled degrees of freedom. Namely, these are the torques applied by the actuation motors of the interlink angles. Since we have assumed that all interlink angles are actuated, the actuation torque vector is given by $\tau = (0 \ 0 \ 0 \ \tau_1 \ \dots \ \tau_{n_L-1})^T$.

2.4 Equations of Motion. Having identified the generalized coordinates and the generalized forces acting on the system, one can take recourse to the Lagrangian formulation to compute the equations of motion. We start by evaluating the Lagrangian which for the above family of mechanical systems is typically defined as the kinetic minus the potential energy. However, since we are focusing our analysis on planar systems, potential energy is assumed constant and thus can be neglected. Hence, the Lagrangian simplifies to

$$\mathcal{L}(q, \dot{q}) = \frac{1}{2} \dot{q}^T \mathcal{M}(q) \dot{q} \quad (6)$$

where $\mathcal{M}(q)$ is the mass matrix associated with the kinetic energy metric. Specifically, for UPM systems, the kinetic energy is given by $\mathcal{L}(q, \dot{q}) = 1/2 \sum_{i=1}^{n_L} (m_i \dot{p}_i^2 + j_i \dot{\alpha}_i^2)$, where \dot{p}_i and $\dot{\alpha}_i$ are the linear and angular velocities of the i th link, respectively. Finally, one can determine the equations of motion by evaluating the Euler–Lagrange equations for $i = 1, 2, \dots, n_L$

$$\frac{d}{dt} \left(\frac{\partial \mathcal{L}(q, \dot{q})}{\partial \dot{q}_i} \right) - \frac{\partial \mathcal{L}(q, \dot{q})}{\partial q_i} + \frac{\partial \mathcal{P}(q, \dot{q})}{\partial \dot{q}_i} = \tau_i \quad (7)$$

2.5 Structure of Equations of Motion. Note that both the Rayleigh power function matrix, $\mathcal{D}(q)$, and the mass matrix, $\mathcal{M}(q)$, that were, respectively, defined in Eqs. (5) and (6) are symmetric matrices. Hence, according to the Lagrangian formulation shown in Ref. [31], the equations of motion (7) governing the dynamics of the system can be expressed in matrix representation such as

$$\mathcal{M}(q) \ddot{q} + C(q, \dot{q}) \dot{q} + \mathcal{D}(q) \dot{q} = \tau \quad (8)$$

where the element in the k th row and j th column of $C(q, \dot{q})$ is defined as $c_{kj} = \sum_{i=1}^n c_{ijk} \dot{q}_i$, where c_{ijk} are the Christoffel symbols of the first kind that are computed by $c_{ijk} = \sum_{l=1}^n \frac{1}{2} \{ (\partial \mathcal{M}_{kl} / \partial q_j) + (\partial \mathcal{M}_{li} / \partial q_k) - (\partial \mathcal{M}_{ij} / \partial q_l) \} \dot{q}_l$.

Given the structure of the configuration space and the nonactuation of the fiber space, the equations of motion in Eq. (8) can be represented in matrix form as follows:

$$\mathcal{M}(q) \begin{pmatrix} \ddot{q} \\ \ddot{r} \end{pmatrix} + C(q, \dot{q}) \begin{pmatrix} \dot{q} \\ \dot{r} \end{pmatrix} + \mathcal{D}(q) \begin{pmatrix} \dot{q} \\ \dot{r} \end{pmatrix} = \begin{pmatrix} 0^{1 \times 1} \\ \tau_i \end{pmatrix} \quad (9)$$

for $i \in \{l+1, l+2, \dots, n\}$. Concentrating on the nonactuated fiber variables, the equations of motion can be expressed as

$$\mathcal{M}^{l \times l}(q) \ddot{q} + \mathcal{M}^{l \times m}(q) \ddot{r} + C(q, \dot{q}) \dot{q} + \mathcal{D}(q) \dot{q} = 0^{1 \times 1} \quad (10)$$

where $\mathcal{M}^{l \times l}(q)$ and $\mathcal{M}^{l \times m}(q)$ are the top left $l \times l$ submatrix and the top right $l \times m$ submatrix of the mass matrix $\mathcal{M}(q)$, respectively. Next, we prove that $\mathcal{M}^{l \times l}(q)$ is nonsingular in the following lemma:

LEMMA 1. Any top left square submatrix of the mass matrix is nonsingular.

Proof. Theorem 2.21 in Ref. [32] states that every principal submatrix of a positive definite is a positive definite matrix. Since $\mathcal{M}^{l \times l}(q)$ is a square submatrix of $\mathcal{M}(q)$, then it is a principal submatrix of $\mathcal{M}(q)$. Hence, $\mathcal{M}^{l \times l}(q)$ is positive definite and thus nonsingular.

Having proved that $\mathcal{M}^{l \times l}(q)$ is nonsingular, we can invert it and use Eq. (10) to solve for the fiber acceleration as follows:

$$\ddot{q} = -(\mathcal{M}^{l \times l}(q))^{-1} (\mathcal{M}^{l \times m}(q) \ddot{r} + C(q, \dot{q}) \dot{q} + \mathcal{D}(q) \dot{q}) \quad (11)$$

Inspecting the right hand side of Eq. (11), one can rewrite it in the following convenient form:

$$\ddot{q} = A_D(q) \dot{q} + A_P(q) \begin{pmatrix} \dot{r} \\ \dot{r} \end{pmatrix} + \frac{1}{2} \dot{q}^T C_R(q) \dot{q} \quad (12)$$

Thus, the fiber accelerations have linear components represented by the linear terms in matrices $A_D(q)$ and $A_P(q)$ as well as cross and quadratic terms represented in the matrix $C_R(q)$. We label the components of matrix $A_D(q)$ as *drift* terms, the components of matrix $A_P(q)$ as *push* terms, and the components of matrix $C_R(q)$ as *cross* terms. The naming of the above matrices, as

well as, the importance of the above structure will be clear in the motion planning section.

2.6 Reduced Equations of Motion. Finally, we take recourse to Lagrangian mechanics to further simplify the equations of motion for UPM systems. Here, we will exploit the fact that the configuration space is a principal fiber-bundle, $Q = G \times M$, and the fact that the fiber space, $G = SE(2)$, is a *Lie group*.

For UPM systems, since we have neglected the potential energy, the Lagrangian is independent on the location of the robot. Technically, the independence of group variables is referred to as G -invariance as was defined in Ref. [33]. This fact, allows us to redefine the Lagrangian in a *reduced* form by exploiting this independence on the fiber variables. Typically, this reduced Lagrangian is computed by doing a coordinate transformation and representing the dynamics in a body-attached coordinate frame. Using similar techniques to the ones in Ref. [34], the reduced Lagrangian has the following form:

$$\tilde{\mathcal{L}}(\xi, r, \dot{r}) = \frac{1}{2} (\xi \quad \dot{r}) \tilde{M}(r) \begin{pmatrix} \xi \\ \dot{r} \end{pmatrix} \quad (13)$$

where ξ is the body velocity as defined in Ref. [35], that is, the velocity of the body-attached coordinate frame as observed from the body-attached coordinate frame and $\tilde{M}(r)$ is the reduced mass matrix. Since, for UPM systems, $G = SE(2)$, the inertial and body fiber velocities are related by the following linear map:

$$\xi = \begin{pmatrix} \cos \theta & \sin \theta & 0 \\ -\sin \theta & \cos \theta & 0 \\ 0 & 0 & 1 \end{pmatrix} \dot{g} \quad (14)$$

The main advantage of expressing the dynamics in terms of the body-attached coordinate frame is the fact that the components of the reduced mass matrix, $\tilde{M}(r)$, are only dependent on the base variables, r_i . Moreover, it has been proven in Ref. [33] that if the Rayleigh dissipation function is G -invariant, then its associated forcing function is G -equivariant. This fact was utilized in Ref. [34] to reduce a G -invariant function, including the Rayleigh dissipation function, to a reduced form. This reduced form is similar in structure to the reduced Lagrangian given in Eq. (13) in the sense that it is independent on the fiber variables. Thus, the reduced Rayleigh dissipation function will have the following form:

$$\tilde{\mathcal{P}}(\xi, r, \dot{r}) = \frac{1}{2} (\xi \quad \dot{r}) \tilde{D}(r) \begin{pmatrix} \xi \\ \dot{r} \end{pmatrix} \quad (15)$$

Using the expressions of the reduced Lagrangian and Rayleigh dissipation function given, respectively, in Eqs. (13) and (15), one can employ similar derivation techniques presented in Ref. [34] to arrive to a reduced set of equations of motion, which can be used to recompute the drift, push, and cross terms to get

$$\dot{\xi} = \tilde{A}_D(r) \xi + \tilde{A}_P(r) \begin{pmatrix} \dot{r} \\ \ddot{r} \end{pmatrix} + \frac{1}{2} (\xi \quad \dot{r}) \tilde{C}_R(r) \begin{pmatrix} \xi \\ \dot{r} \end{pmatrix} \quad (16)$$

Here, $\dot{\xi}$ represents the fiber accelerations computed in Eq. (12); however, now the accelerations are computed in the body-attached coordinate frame. It is worth noting that in the above reduced equations of motion, the drift, push, and cross terms are only a function of the base variables, r_i .

3 Motion Planning

In this section, we exploit the special structure of the equations of motion for the UPM systems as well as a specially designed family of allowable inputs to solve the motion planning problem.

This motion planning solution not only will specify the interlink inputs but also the location of the friction pads along the individual links, that is, we design the gaits for motion planning problems as well as set some geometric parameters of the system itself.

3.1 Proposed Inputs. In this paper, the underactuation of the system is realized by assuming full control over solely the base or shape variables, r_i . Hence, while solving the motion planning problem, one does not utilize the base variables' dynamics, which are given by the last l equations in Eq. (9).

Moreover, we limit our base variable trajectories to be composed of only two types of curves: an *active* segment where the input variables are allowed to change in a desired way and a *locked* segment where all the base input variables are locked at their current position. Figure 2 depicts a possible input comprised of two active segments and three locked segments. In the active regions, the value of the input, r_i , changes first from A to B and then back to A whereas in the locked regions, the input r_i maintains a constant value.

At the interface between the active and locked segments, it is assumed that the time derivatives, up to second order, of all the base variable trajectories are zero. This can be clearly seen in Fig. 2 where the first and second derivatives are also depicted. Thus, one potential analytic representation for the input variables is to use *sigmoid* functions such as

$$f_{a,b,A,B,s}(t) = \begin{cases} A & \text{if } t \leq a \\ \frac{B-A}{1+e^{\frac{1}{s}(t-a)}} & \text{if } a < t < b \\ B & \text{if } t \geq b \end{cases} \quad (17)$$

The above expression is used to construct the input shown in Fig. 2, where a , b , A , B , and s are real positive numbers that represent the parameters of this function. a and b denote the start and end of the active segments of the curve, A and B denote the values of the locked segments adjacent to the active segment, and s is a parameter setting the slope of the curve in the middle of the active segment.

DEFINITION 3. *The smallest subsegment of an allowable gait for all the base variables must be composed of the following sequence of five adjacent sections: locked, active, locked, active, and locked such that the first and last locked sections have the same value, which is different from the middle locked section. Moreover, the graphs of the active sections are mirrored about a vertical line located at the midpoint of the middle locked section.*

Mathematically, the smallest subsegment of an allowable gait is given by

$$F_{a,b,A,B,s,\kappa}(t) = f_{a,b,A,B,s}(t) - f_{a,b,A,B,s}(t - \kappa) \quad (18)$$

where $\kappa > b$ is a time shifting parameter. Using the above defined allowable gait segments similar to the one shown in Fig. 2, the

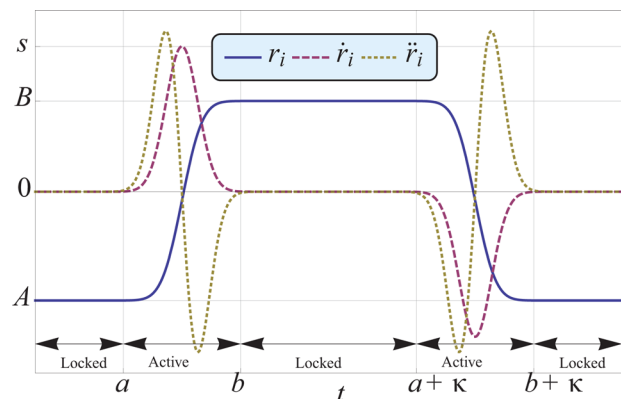


Fig. 2 An allowable input, $r_i = f_{a,b,A,B,s}(t) - f_{a,b,A,B,s}(t + \kappa)$

following conditions are deduced: each subsegment is cyclic, the entire input is cyclic, and two adjacent subsegments can share the same locked portion. Next, we define the reverse of an input.

DEFINITION 4. For a given base variables input, $r_i = F_i(t)$, for all $i = 1, 2, \dots, m$, the associated reverse input is defined as $\bar{r}_i = -F_i(t)$ for all $i = 1, 2, \dots, m$.

3.2 Motion Planning Analysis. In this section, we solve the motion planning problem by utilizing both the structure of the equations of motion for UPM systems which was depicted in Eq. (16) and the specially design family of inputs depicted in Eq. (18). We start by investigating the locomotion of UPM systems for any input and its reverse. That is, we want to analyze the time evolution of the fiber variables, g , for an input, r , and its reverse, \bar{r} . Without any loss of generality, we shall assume that the system starts from rest, that is, at $t=0$, the body-attached frame is coincident with the inertial fixed frame such that, $g(0) = \dot{g}(0) = (0, 0, 0)^T$. We start the motion planning analysis by the following lemma:

LEMMA 2. Given a UPM system in a viscous environment, the time evolution of the fiber variables, g_i , for an input, r versus its reverse, \bar{r} , is either identical or the reverse of g_i , that is

$$g_i(\bar{r}) = \pm g_i(r), \text{ for all } i = 1, 2, \dots, l \quad (19)$$

Proof. The only external forces acting on the system are viscous frictional forces that are linearly related to the generalized velocities. Thus, once the inputs are reversed, all the forces reverse direction. Assume that the all the forces produce a net force and net torque about the system's center mass. As soon as the inputs are reversed, the net force and torque will change direction, but the magnitude remains unchanged.

Hence, if the system is starting from rest, one can conclude $\theta(r) = -\theta(\bar{r})$. However, for the x and y directions of motion, the relation will depend on the alignment of the body-attached coordinate frame. Since, we aligned the first axis of the body-attached frame along the average of the absolute link angles, we conclude that $x(r) = \pm x(\bar{r})$ and $y(r) = \pm y(\bar{r})$. Hence, we conclude that $g_i(\bar{r}) = \pm g_i(r)$ for $g_i \in \{x, y, \theta\}$.

Given the above lemma, one can deduce the same relationship among the fiber accelerations, that is, $\dot{g}_i(\bar{r}) = \pm \dot{g}_i(r)$ and $\ddot{g}_i(\bar{r}) = \pm \ddot{g}_i(r)$ for all $i = 1, 2, \dots, l$. Moreover, using the relation in Eq. (14) between the fiber velocity, \dot{g} , and its representation in the body-attached frame, ξ , one can deduce similar conditions on ξ . Specifically, for the fiber space $G = \text{SE}(2)$, we have $\xi_i(\bar{r}) = \pm \xi_i(r)$ and $\ddot{\xi}_i(\bar{r}) = \pm \ddot{\xi}_i(r)$ for all $i = 1, 2, \dots, l$.

For UPM systems, since $G = \text{SE}(2)$ is three-dimensional, we have a total of 2^3 or eight choices for the relationship depicted in Eq. (19). Each of these choices should be checked if it is compatible with the equations of motion given in Eq. (16). At the core of our proposed motion planning analysis is checking which of the all the possible choice is consistent with the equations of motion.

PROPOSITION 1. For a UPM system in a viscous environment, the relationship between the evolution of fiber variables for an allowable input as defined in Eq. (18) and its reverse is given by

$$\xi_x(r) = \xi_x(\bar{r}), \xi_y(r) = -\xi_y(\bar{r}), \text{ and } \xi_\theta(r) = -\xi_\theta(\bar{r}) \quad (20)$$

Proof. In Lemma 2, it was proven that $\xi_\theta(r) = -\xi_\theta(\bar{r})$; however, for the other two fiber variables, we have $\xi_x(r) = \pm \xi_x(\bar{r})$ and $\xi_y(r) = \pm \xi_y(\bar{r})$. Without loss of generality, one can align the axes of the body-attached frame such that $\xi_x(r) = +\xi_x(\bar{r})$ and $\xi_y(r) = -\xi_y(\bar{r})$.

This final proven relationship, depicted in Eq. (20), relating the motion of a UPM along each of the fiber variables due to an input and its reverse is at the basis of our proposed motion planning solution. In fact, this relationship will be exploited to design the gaits and specify the friction pads location in order to produce a desired motion of the system. Next, we work out a

two-link UPM example, for which we determine all the expressions that were introduced in this section as well as we validate all the relevant lemmas and ultimately solve its motion planning problem.

4 Motion Planning for Two-Link System

In this section, we solve the motion planning problem for the two-link, $n_L = 2$, UPM system depicted in Fig. 1. We assume that the links are identical as well as the frictional properties of the friction pads; however, the location of the friction pads along the links could be different for each link. Moreover, for simulation results, we will use the following parameters:

$$M = 1; J = \frac{1}{12}; L = 1; d = \pm 1, \nu = 1, \mu = \frac{1}{2} \quad (21)$$

4.1 Equations of Motion. Before we address the motion planning problem, we work out the equations of motion for a two-link example from the family of underactuated systems. Using the suggested generalized coordinate approach in Eqs. (1) and (2), the body-frame is located as shown in Fig. 1. For this two-link example, the generalized coordinates vector is given by $q = (x \ y \ \theta \ \phi_1)^T$, and one can determine the kinetic energy as $\mathcal{L}(q, \dot{q}) = M(\dot{x}^2 + \dot{y}^2) + \left(J + M(L \cos \phi_1)^2 \right) \dot{\theta}^2 + \left(J + M(L \sin \phi_1)^2 \right) \dot{\phi}_1^2$.

For evaluating the frictional forces, we start by computing the velocity components parallel and perpendicular to the links at the friction pads. For the two-link system, these components are

$$\begin{pmatrix} v_1^{\parallel} \\ v_2^{\parallel} \\ v_1^{\perp} \\ v_2^{\perp} \end{pmatrix} = \begin{bmatrix} c_{\theta-\phi_1} & s_{\theta-\phi_1} & \frac{L}{2}s_{2\phi_1} & \frac{L}{2}s_{2\phi_1} \\ c_{\theta+\phi_1} & s_{\theta+\phi_1} & \frac{L}{2}s_{2\phi_1} & -\frac{L}{2}s_{2\phi_1} \\ -s_{\theta-\phi_1} & c_{\theta-\phi_1} & d_1 - Lc_{\phi_1}^2 & -d_1 + Ld_{\phi_1}^2 \\ -s_{\theta+\phi_1} & c_{\theta+\phi_1} & d_2 + Ls_{\phi_1}^2 & d_2 + Ld_{\phi_1}^2 \end{bmatrix} \begin{pmatrix} \dot{x} \\ \dot{y} \\ \dot{\theta} \\ \dot{\phi}_1 \end{pmatrix}$$

Here, we have used a short-hand notation for the trigonometric functions, that is, $c_{\alpha \pm b \beta}^p = (\cos(\alpha x \pm b \beta))^p$ and $s_{\alpha \pm b \beta}^p = (\sin(\alpha x \pm b \beta))^p$. Using the above velocity components, one can compute the Rayleigh power function, $\mathcal{P}(q, \dot{q})$. Then, one can use Eq. (7) to determine the equations of motion governing the locomotion of the two-link system.

4.2 Structure of Equations of Motion. Utilizing the equations for motion from Eq. (7), one can first solve for the accelerations of the fiber variables, \ddot{g} . Then by using the change of variables which is given in Eq. (14), one can represent these accelerations in the body-attached coordinate frame. Thus, solving for the accelerations, $\ddot{\xi}$, one can use Eq. (16) to evaluate the drift, push, and cross term to get

$$\tilde{A}_D(q) = \begin{bmatrix} x\gamma_x & x\gamma_y & x\gamma_\theta \\ y\gamma_x & y\gamma_y & y\gamma_\theta \\ \theta\gamma_x & \theta\gamma_y & \theta\gamma_\theta \end{bmatrix}, \tilde{A}_P(q) = \begin{bmatrix} x\gamma_{\phi_1} \\ y\gamma_{\phi_1} \\ \theta\gamma_{\phi_1} \end{bmatrix}, \tilde{C}_r(q) = \begin{bmatrix} x\gamma_{\phi_1\theta} \\ y\gamma_{\phi_1\theta} \\ \theta\gamma_{\phi_1\theta} \end{bmatrix} \quad (22)$$

where we have

$$\begin{aligned} x\gamma_x &= -\frac{1}{M}(\nu c_{\phi_1}^2 + \mu s_{\phi_1}^2) \\ x\gamma_y &= 0 \\ x\gamma_\theta &= \frac{s_{\phi_1}}{2M}(\mu(-d_1 + d_2 + 2L) - 2Lc_{\phi_1}^2(\mu + \nu)) \\ x\gamma_{\phi_1} &= \frac{\mu s_{\phi_1}}{2M}(d_1 + d_2) \\ x\gamma_{\phi_1\theta} &= 0 \end{aligned}$$

$$\begin{aligned}
\begin{matrix} y\gamma_x \\ y\gamma_y \end{matrix} &= \mathbf{0} \\
y\gamma_y &= -\frac{1}{M}(\mu c_{\phi_1}^2 + \nu s_{\phi_1}^2) \\
y\gamma_\theta &= -\frac{\mu c_{\phi_1}}{2M}(d_1 + d_2) \\
y\gamma_{\phi_1} &= \frac{c_{\phi_1}}{2M}(\mu(-2Lc_{\phi_1}^2 + d_1 - d_2) + 2L\nu s_{\phi_1}^2) \\
y\gamma_{\phi_1\theta} &= 0 \\
o\gamma_x &= \frac{s_{\phi_1}}{2J + 2ML^2s_{\phi_1}^2}((d_2 - d_1)\mu + 2L(\mu - \nu)s_{\phi_1}^2) \\
o\gamma_y &= -\frac{\mu c_{\phi_1}}{2J + 2ML^2s_{\phi_1}^2}(d_1 + d_2) \\
o\gamma_\theta &= -\frac{\mu}{2(J + L^2Ms_{\phi_1}^2)}(d_1^2 + d_2^2) \\
&\quad - \frac{Ls_{\phi_1}^2}{(J + L^2Ms_{\phi_1}^2)}((\mu(d_2 - d_1) + L\nu) + (\mu - \nu)s_{\phi_1}^2) \\
o\gamma_{\phi_1} &= -\frac{(d_1 + d_2)\mu(-d_1 + d_2 + L)}{2(J + L^2Ms_{\phi_1}^2)} \\
o\gamma_{\phi_1\theta} &= \frac{2L^2Mc_{\phi_1}s_{\phi_1}}{J + L^2Ms_{\phi_1}^2}
\end{aligned}$$

From the above expressions, as expected the components of the drift, push, and cross terms are independent of any fiber variables, x , y , and θ , and only depend on the base variable, ϕ_1 .

4.3 Motion Planning Analysis. Recalling the two-link example the base space is one-dimensional, $m=1$. To validate that Proposition 1 provides that only compatible equations of motion, we simulate the system with two inputs, $\phi_1(t) = f_{0.5,5.5,0.2,5}(t)$ and its reverse $\bar{\phi}_1(t) = -f_{0.5,5.5,0.2,5}(t)$. The plots for ϕ_1 and $\bar{\phi}_1$ are shown Fig. 3. As for the rest of the fiber variables, it is clear from Fig. 3 that $x(\phi_1) = x(\bar{\phi}_1)$ while $y(\phi_1) = -y(\bar{\phi}_1)$ and $\theta(\phi_1) = -\theta(\bar{\phi}_1)$.

To validate that this is indeed the only compatible choice for the equations of motion, we compute and compare the left-hand-side and the right-hand-side of Eq. (16). To simplify some expressions, we use the *hat* operator to refer to the following ratio:

$$\hat{f} = \frac{f(r)}{f(\bar{r})} \quad (23)$$

Accordingly, one can compare the accelerations, $\hat{\xi}_x$, $\hat{\xi}_y$, and $\hat{\xi}_\theta$, of the two-link example, expressed in the body-frame, for an input r

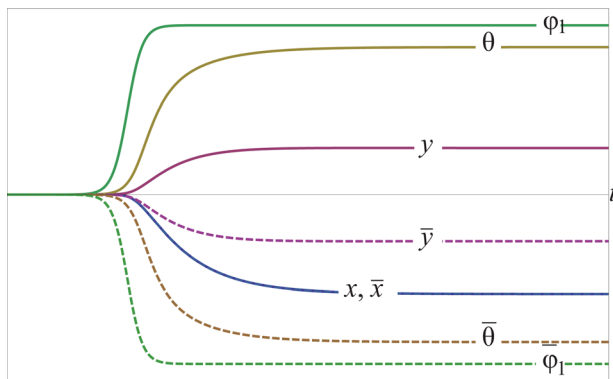


Fig. 3 Numerical simulation for the two inputs, $\phi_1(t) = f_{0.5,5.5,0.2,5}(t)$ and its reverse $\bar{\phi}_1(t) = -f_{0.5,5.5,0.2,5}(t)$

and its reverse \bar{r} . This is done by inspecting the drift, push, and cross terms for the planar mechanical system, which for the two-link example we listed in Sec. 4.2. For all possible choices computed in Lemma 2, one would evaluate $x\hat{\gamma}_i$ and its coefficients for an input and its reverse. A valid choice would have the left-hand-side and the right-hand-side of all equations matching. Indeed we were able to verify that the *only* valid choice is $\hat{\gamma}_x = \hat{\xi}_x = 1$, $\hat{\gamma}_y = \hat{\xi}_y = -1$, and $\hat{\gamma}_\theta = \hat{\xi}_\theta = -1$ which is consistent with the result of Proposition 1. One can also check the push, drift, and cross terms. If all the right-hand terms, after multiplication, are the same as the left hand terms while ignoring all zeros, then the choice is valid.

The above analysis for this particular choice is depicted in Table 1. Referring back to Fig. 3, one can see that for an input and its reverse, the time evolution for x is identical, whereas the time evolution for y and θ are reversed. Moreover, note that the input, ϕ_1 , is reversed by design.

Next, we solve the motion planning problem for the two-link system. We accomplish this by exploiting the simplified set of equations of motion that were derived earlier. The proposed motion planning solution to locomote the system along an unactuated degree of freedom not only specifies the gaits or inputs to the actuated degrees of freedom but also the location of the friction pads in the system. Thus, our motion planning solution can be used as a gait evaluation tool as well as a system design tool.

4.4 Locomotion Along y . The ideal trajectory for locomotion solely along the y direction in a planar environment is for the center of mass to trace a line parallel to the y axis. That is, the acceleration along the other degrees of freedom, namely, x and θ , must be zero for all time. To achieve this, taking recourse to the equations of motion in Eq. (16), one needs to nullify the push and cross terms for the x and θ equation. That is, one needs to impose the following conditions $x\gamma_y = x\gamma_{\phi_1} = x\gamma_{\phi_1\theta} = 0$ and $o\gamma_y = o\gamma_{\phi_1} = o\gamma_{\phi_1\theta} = 0$.

With the above condition satisfied, the equations of motion reduce to

$$\begin{pmatrix} \ddot{x} \\ \ddot{y} \\ \ddot{\theta} \end{pmatrix} = \begin{bmatrix} x\gamma_x & 0 & x\gamma_\theta & 0 & 0 \\ 0 & y\gamma_y & y\gamma_\theta & y\gamma_{\phi_1} & 0 \\ o\gamma_x & 0 & o\gamma_\theta & 0 & 0 \end{bmatrix} \begin{pmatrix} \dot{x} \\ \dot{y} \\ \dot{\theta} \\ \dot{\phi}_1 \\ \dot{\phi}_1\dot{\theta} \end{pmatrix} \quad (24)$$

Note that the first and third equations are coupled with zero initial condition, hence both x and θ remain zero for all time. This is true, since the coefficients for the forcing functions are all zero.

4.4.1 Friction Pads Location. Utilizing the above conditions and equating the relevant terms to zero, we get

$$\begin{aligned}
0 &= x\gamma_{\phi_1} = \frac{\mu s_{\phi_1}}{2M}(d_1 + d_2) \\
0 &= o\gamma_y = -\frac{\mu c_{\phi_1}}{2J + 2ML^2s_{\phi_1}^2}(d_1 + d_2)
\end{aligned}$$

Table 1 The only valid choice for the two-link example

	$x\hat{\gamma}_x$	$\hat{\xi}_x$	$x\hat{\gamma}_y$	$\hat{\xi}_y$	$x\hat{\gamma}_\theta$	$\hat{\xi}_\theta$	$x\hat{\gamma}_{\phi_1}$	$\dot{\phi}_1$	$x\hat{\gamma}_{\theta\phi_1}$	ξ_θ	$\dot{\phi}_1$
$\hat{\xi}_x$	1	1	-1	-1	-1	-1	-1	-1	0	-1	-1
1	1		1		1		1		0		
	$y\hat{\gamma}_x$	$\hat{\xi}_x$	$y\hat{\gamma}_y$	$\hat{\xi}_y$	$y\hat{\gamma}_\theta$	$\hat{\xi}_\theta$	$y\hat{\gamma}_{\phi_1}$	$\dot{\phi}_1$	$y\hat{\gamma}_{\theta\phi_1}$	ξ_θ	$\dot{\phi}_1$
$\hat{\xi}_y$	-1	1	1	-1	1	-1	1	-1	0	-1	-1
-1	-1		-1		-1		-1		0		
	$o\hat{\gamma}_x$	$\hat{\xi}_x$	$o\hat{\gamma}_y$	$\hat{\xi}_y$	$o\hat{\gamma}_\theta$	$\hat{\xi}_\theta$	$o\hat{\gamma}_{\phi_1}$	$\dot{\phi}_1$	$o\hat{\gamma}_{\theta\phi_1}$	ξ_θ	$\dot{\phi}_1$
$\hat{\xi}_\theta$	-1	1	1	-1	1	-1	1	-1	-1	-1	-1
-1	-1		-1		-1		-1		-1		

$$0 = {}_{\theta} \gamma_{\phi_1} = -\frac{(d_1 + d_2)\mu(-d_1 + d_2 + L)}{2(J + L^2 M s_{\phi_1}^2)}$$

$$0 = {}_{\theta} \gamma_{\phi_1 \theta} = \frac{2L^2 M c_{\phi_1} s_{\phi_1}}{J + L^2 M s_{\phi_1}^2}$$

The solution that ensures the first three conditions are satisfied is given by

$$d_1 = -d_2 \quad (25)$$

This solution specifies the location of the friction pads. Referring to Fig. 1, this above configuration refers to symmetric robots, that is, the friction pads are located at the same distance away from the interlink joint.

As for the fourth condition, that is, setting the cross term, ${}_{\theta} \gamma_{\phi_1 \theta} = 0$, recall that this term multiplies the variables $\dot{\phi}_1 \dot{\theta}$. Since, we are starting from rest, we have $\dot{\theta}(t=0) = 0$. Thus, this cross term does not affect the rotational acceleration at $t=0$. Accordingly, the two degrees of freedom x and θ are coupled and since there are no forcing functions, they remain identically zero for all time.

4.4.2 Gait Analysis. Having, identified the location of the friction pads that ensures no motion along x and θ , we focus our analysis on the y degree of freedom. Plugging the symmetric configuration parameters from Eq. (25) into the y equation of motion, we get

$$\ddot{y} + \Gamma_d \dot{y} = \Gamma_p \dot{\phi}_1, \text{ where}$$

$$\Gamma_d = \frac{\mu}{M} \left(c_{\phi_1}^2 + \frac{\nu}{\mu} s_{\phi_1}^2 \right),$$

$$\Gamma_p = -\frac{\mu L c_{\phi_1}}{M} \left(\frac{d}{L} - \left(\frac{\nu}{\mu} - 1 \right) c_{\phi_1}^2 \right), \text{ and}$$

$$d = -d_1 = d_2 \quad (26)$$

Recall that the terms Γ_d and Γ_p are the drift and push terms, respectively.

Now, we analyze this equation of motion when the input is limited to the set of allowable gaits described in Sec. 3.1. For the *locked* portion of the input, that is, $\dot{\phi}_1 = 0$, the effect of the push term, Γ_p , vanishes. Given that friction coefficients are positive, then the drift term, Γ_d , is positive for any input. For this case, if the system has any initial velocity along y , this velocity will decay exponentially with a time constant equivalent to the reciprocal of the drift term, $\tau_d = 1/\Gamma_d$. This makes sense since the viscous friction will dissipate the initial energy in the system. For all practical purposes, the system should dissipate energy for at least five multiples of the system's time constant. Thus, the minimum duration of the locked sections of the input are bounded by $T_d \geq 5(\tau_d = 1/\Gamma_d)$.

As for the *active* sections of the input gait, assuming the worst case scenario where the system is starting from rest, that is, $\dot{y} = 0$. This will nullify the effect of drift term, Γ_d . By design, for the active section of the gait, the first derivative of the input gait is greater than zero as seen in Fig. 2. Thus, to maximize the effect of the push, the sign of the push term should remain the same during the entire active section of the gait.

This above fact can be used to actually design gaits. In Fig. 4, we plot the boundaries for which the push, Γ_p , term changes sign. For instance, if a robot's parameters are such that, $d/L = -1/3$ and the ratio of the coefficients of friction is such that $\nu/\mu = 1/2$, then the maximum allowed value for the input angle is $\phi(t) \leq \phi_{\text{allowable}}$, as depicted in Fig. 4.

4.4.3 Gait Design. In this section, we will utilize the gait analysis in Sec. 4.4.2 to actually design a gait that moves the two-link system along the global y direction. Using the system parameters given in Eq. (21), we have $d/L = 1$. Using Fig. 4, it is clear

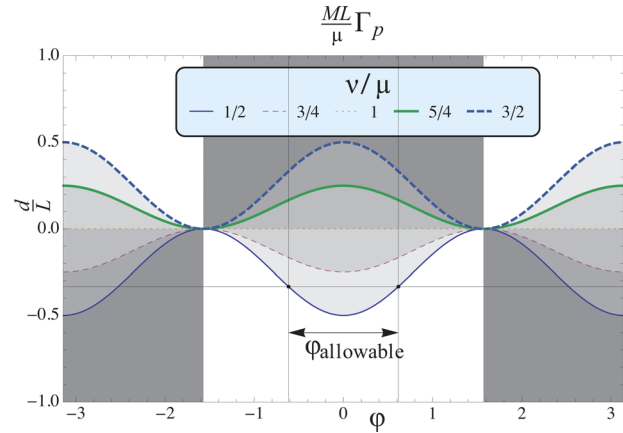


Fig. 4 Same signed regions for the push term Γ_p

that the input angle $|\phi_1| \leq \pi/2$ so that the push term maintains the same sign. Now consider the following gait:

$$\phi_1(t) = F_{0.5,0.1,5,15}(t) \quad (27)$$

Using Eq. (18), the active sections are 5 s long and the locked sections are 10 s long. This input gait is depicted by the dashed-dotted line in Fig. 5. Also note that $\phi_1(t) < \pi/2$.

So starting from a straight configuration and from rest, the gait is comprised of five sections: locked, active, locked, active, and locked. The first locked section is for $t < 0$. For the range of input, the maximum value for the drift term is $\Gamma_p \leq 2.0$; hence, for the duration of the locked sections should be $T \geq 10.0$ s. The proposed gait in Eq. (27) satisfies this condition since the length of the locked sections is 10 s. Also note that the active sections change the input angle from 0 to a maximum value of 1 and back to 0. Finally, for this input, one can verify that the drift term, Γ_d , is always positive while the push term, Γ_p , remains negative for the entire gait.

4.4.4 Locomotion Analysis. Let $g_i \Delta$ be the net change in position along the $g_i \in \{x, y, \theta\}$ direction due to the input gait $\phi_1(t)$ given in Eq. (27). In Secs. 4.4.1 and 4.4.2, we proved that the system does not translate along x nor does it rotate. Thus, we have $x\Delta = \theta\Delta = 0$. Next, we need to verify that the system actually translates along the y direction for the proposed gait.

To simplify the analysis, we partition the input gait into two sections of equal duration. Define the net motion for each section as follows: ${}_y \Delta_a = y(15) - y(0)$ and ${}_y \Delta_b = y(30) - y(15)$. For a non-zero net motion along y , we must have ${}_y \Delta \neq 0$ or in other words, ${}_y \Delta_a + {}_y \Delta_b \neq 0$. For the gait above, as depicted by the solid line in Fig. 5, the active section of ϕ_a spans the duration between 0 and 5 s while the active section of ϕ_b spans the duration between 15 and 20 s.

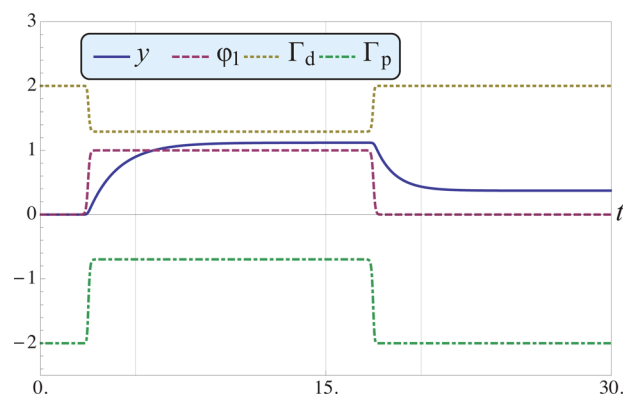


Fig. 5 The evolution of y , ϕ_1 , the push term, and the drift term for the two-link system

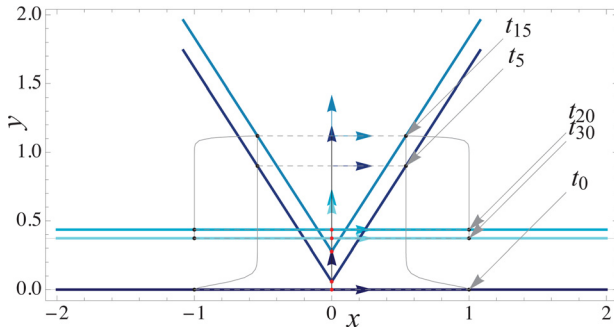


Fig. 6 Net motion along the y of the two-link system, $t_i \Leftrightarrow (t = i \text{ sec})$

Moreover, since the locked section between the two active sections is 10 s long, for all practical purposes, the second active section is the reverse of the first active section. The only difference between these sections is the starting shape of the two-link system. The first active section changes the interlink angle from 0 to 1 while the second active section changes this angle from 1 back to 0. Indeed, it is this change in the starting shape, coupled with the nonisotropic friction that causes the difference between the effect of the active gaits' sections and the motion along the y direction. This difference is depicted by the dashed line in Fig. 5 where the net motion along the y direction at the end of the gait is $y\Delta = 0.372$. Also note, as expected, the exponential behavior of y versus t for the locked sections of the gait.

A trace of the two-link system is depicted in Fig. 6 as the proposed gait is being simulated. The system starts from the origin with a straight configuration, that is, $\phi_1 = 0$. Then, the system folds in during the active section from t_0 till t_5 and then drifts through the locked section till t_{15} , it reaches rest again but at the folded configuration. Finally, the system unfolds back to the straight configuration and the net displacement along the y direction is depicted. This is due to the drift term, dotted line in Fig. 5, being higher in the second section, thus shortening the motion along y , that is, $y\Delta_a > y\Delta_b$.

We have also simulated an underactuated system using the WEBOTS modeling and simulation software. The interaction between the robot and the fluid was defined as a viscous interaction. Inputting the above gait into the system yields identical motion similar to the motion explained above. The top grid of frames in Fig. 7 depicts the sequence of shape changes that the robot undergoes while performing the gait while the bottom image depicts a trace of the center of mass after performing several cycles of the proposed gait. Note that as expected, the robot locomotes along the y direction without any motion along the other fiber variables, x and θ .

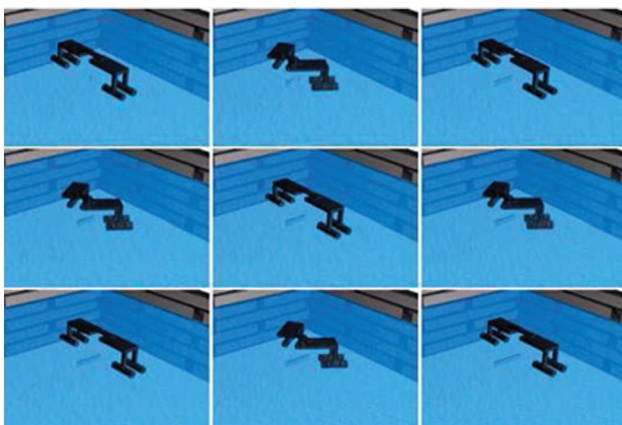


Fig. 7 Simulation using WEBOTS depicting motion along y

4.5 Locomotion Along x . Similar to the vertical locomotion case, the ideal trajectory for horizontal locomotion in a planar environment is for the center of mass to trace a horizontal line. That is, the acceleration along the other degrees of freedom, namely, y and θ , must be zero for all time. To achieve this, taking recourse to the equations of motion in Eq. (16), one needs to simultaneously nullify the push and cross terms for the y and θ equation. That is, one needs to impose the following conditions: $y\ddot{y} = \dot{y}\dot{\phi}_1 = \dot{y}\dot{\phi}_1\theta = 0$, $\theta\dot{\gamma}_y = \theta\dot{\gamma}_{\phi_1} = \theta\dot{\gamma}_{\phi_1\theta} = 0$.

Unfortunately, there exists no solution that will simultaneously satisfy the above conditions. Hence, the structure of the equations of motion is unmodified and is given by

$$\begin{pmatrix} \ddot{x} \\ \ddot{y} \\ \ddot{\theta} \end{pmatrix} = \begin{bmatrix} x\gamma_x & 0 & x\gamma_\theta & x\gamma_{\phi_1} & 0 \\ 0 & y\gamma_y & y\gamma_\theta & y\gamma_{\phi_1} & 0 \\ \theta\gamma_x & \theta\gamma_y & \theta\gamma_\theta & \theta\gamma_{\phi_1} & \theta\gamma_{\phi_1\theta} \end{bmatrix} \begin{pmatrix} \dot{x} \\ \dot{y} \\ \dot{\theta} \\ \dot{\phi}_1 \\ \dot{\phi}_1\dot{\theta} \end{pmatrix} \quad (28)$$

4.5.1 Location of the Friction Pads. The next best recourse to achieve motion along the x direction is to nullify the motion along the other degrees of freedom over the course of several inputs while additively locomoting along the x direction. Moreover, since one would want to maximize the motion along x , the push term along the x direction should be maximized. Inspecting the push term, $x\gamma_{\phi_1}$, in Sec. 4.2, it is maximized by setting

$$d_1 = d_2 \quad (29)$$

The above condition for the location of the friction pads indicate that the links of the two-link system are identical, that is, the friction pads are equidistant from the links' centers of mass and one the same side of the centers of mass.

4.5.2 Gait Analysis. Similar to the earlier analysis, the gaits will be comprised of active and locked sections. The active sections are the sections where $\dot{\phi}_1 \neq 0$ and for each active section $\dot{\phi}_1$ does not change sign. As for the locked sections, we have $\dot{\phi}_1 = 0$. Moreover, the duration of the locked sections are related to the drift terms. Since each of the degrees of freedom has its own time constant, we should take the maximum time constant for all degrees of freedom to ensure that the system has come to rest at the end of each locked section. For the condition given in Eq. (29), the drift terms are denoted by the diagonal terms of the following matrix:

$$A_D(q) = \begin{pmatrix} \frac{(\nu - \mu)s_{\phi_1}^2 - \nu}{M} & 0 & \frac{Ls_{\phi_1}((\mu + \nu)s_{\phi_1}^2 - \nu)}{M} \\ 0 & \frac{(\mu - \nu)s_{\phi_1}^2 - \mu}{M} & \frac{d\mu c_{\phi_1}}{M} \\ \frac{L(\mu - \nu)s_{\phi_1}^3}{L^2Ms_{\phi_1}^2 + J} & \frac{d\mu c_{\phi_1}}{L^2Ms_{\phi_1}^2 + J} & \frac{\mu d^2 + L^2s_{\phi_1}^2(\nu c_{\phi_1}^2 + \mu s_{\phi_1}^2)}{L^2Ms_{\phi_1}^2 + J} \end{pmatrix}$$

A plot of the drift terms is depicted in Fig. 8. In order to estimate the time constant for each of the degrees of freedom, we compute the average value of the drift term for the entire range of $|\phi_1| \leq \pi$. This average value is equivalent to dividing the area under each drift term and then dividing it by the length of the range, that is, 2π . For the parameter set given in Eq. (21), the estimate of the time constants is given by $x\bar{\gamma}_x = 3.91rd$, and $y\bar{\gamma}_y = \theta\bar{\gamma}_\theta = 0.75rd$. Thus, the locked portion of a proposed gait of a duration of 10 s should be adequate.

4.5.3 Gait Design. The proposed gait will have at least 16 sections, eight locked sections, and eight active sections. The proposed gait is given by

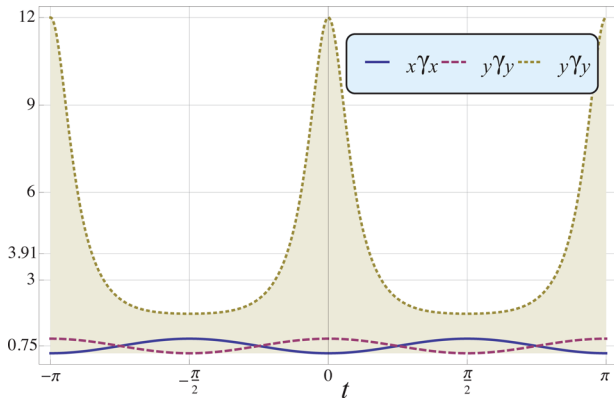


Fig. 8 The drift terms of the two-link system

$$\begin{aligned} \phi_1(t) = & F_{0,5,0,1,5,15}(t) - F_{0,5,0,1,5,15}(t - 30) \\ & - F_{0,5,0,1,5,15}(t - 60) + F_{0,5,0,1,5,15}(t - 90) \end{aligned} \quad (30)$$

This gait is defined using Eq. (18) and is depicted by the dashed and dotted line in Fig. 9. Starting from rest and from the straight configuration, the gait will change the interlink angle to a certain value, back to zero, to a negative value, back to zero, then the entire sequence is mirrored. The absolute value of the nonzero values of the interlink angles are identical. For this particular gait, we chose the nonzero value of the interlink angle to be $|\phi_1| \leq 1rad$.

Accordingly, we can divide the proposed gait into four composite sections, each having two active and two locked sections. Label the net motion along each degree of freedom $g_i \in \{x, y, \theta\}$ as follows:

$$\begin{aligned} g_i \Delta_a &= g_i(30) - g_i(0), & g_i \Delta_b &= g_i(60) - g_i(30), \\ g_i \Delta_c &= g_i(90) - g_i(60), & g_i \Delta_d &= g_i(120) - g_i(90) \end{aligned}$$

In Sec. 4.5.4 we shall verify that the proposed gait causes the two-link system to move solely along the x direction while restoring the other two degrees of freedom, y and θ back to their initial values once the gait is completed.

4.5.4 Locomotion analysis. Without loss of generality, assume that the first subsection actually changes all three degrees of freedom, that is, ${}_x\Delta_a \neq 0$, ${}_y\Delta_a \neq 0$, and ${}_\theta\Delta_a \neq 0$. At the end of this portion of the gait, at 30 s, the system comes to rest. The next portion of the gait is the reverse of the first portion. Thus, we know for a fact that ${}_x\Delta_b \neq -{}_x\Delta_a$, ${}_y\Delta_b \neq -{}_y\Delta_a$, and ${}_\theta\Delta_b = -{}_\theta\Delta_a$. This is due to the fact that the starting orientation is different for each subsection, this conclude that

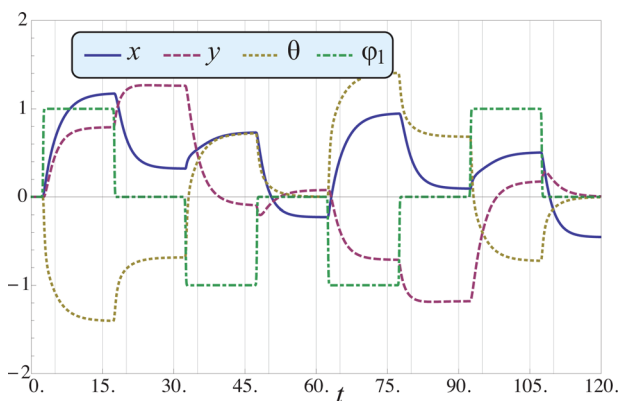


Fig. 9 The evolution of the degrees of freedom for the two-link system

$${}_x\Delta_a + {}_x\Delta_b \neq 0, \quad {}_y\Delta_a + {}_y\Delta_b \neq 0, \quad \text{and} \quad {}_\theta\Delta_a + {}_\theta\Delta_b = 0$$

Hence, at $t = 60$ s, the two-link system has a straight configuration, its orientation is restored to the initial orientation, and it has translated along both the x and y direction. This can be seen in Fig. 10.

To eliminate the undesired motion along the y direction, the reverse of the two subsections is applied. Since, we are starting from a straight configuration and from a similar orientation, we have the following:

$$\begin{aligned} {}_x\Delta_a + {}_x\Delta_b &= {}_x\Delta_c + {}_x\Delta_d, \\ {}_y\Delta_a + {}_y\Delta_b &= -({}_y\Delta_c + {}_y\Delta_d), \\ {}_\theta\Delta_a + {}_\theta\Delta_b &= {}_\theta\Delta_c + {}_\theta\Delta_d = 0 \end{aligned}$$

Hence, after completing the entire proposed gait in Eq. (30), we have ${}_x\Delta = -0.452$ while ${}_y\Delta = {}_\theta\Delta = 0$. Thus, the proposed gait guarantees that the system only translates along the x direction after the completion of the entire gait. The motion along all the degrees of freedom is depicted in Fig. 9. A trace of the two-link system as it performs the proposed gait is shown in Fig. 10 where the position and shape of the system are depicted at the end of each section of the gait.

Again, the above gait was implemented using the simulation software WEBOTS. The resulting motion is depicted in Fig. 11. The top grid of frames shows the series of shape changes that represent the implemented gait while the bottom image depicts a trace of the center of mass after performing several cycles. It is clear that the overall motion is along the x direction even though, as expected, there is intermediate motion along the other fiber variables, y and θ .

4.6 Motion Versus the Roller Racer. Finally, in this section, we compare the motion of the two-link robot to that of a roller racer with comparable parameters. Recall that the roller racer is comprised of two-link but instead of having friction pads it has passive rolling wheels. The assumption that the wheels do not slide sideways and do not have any rolling friction provides non-holonomic constraints on the system. For our simulation purposes,

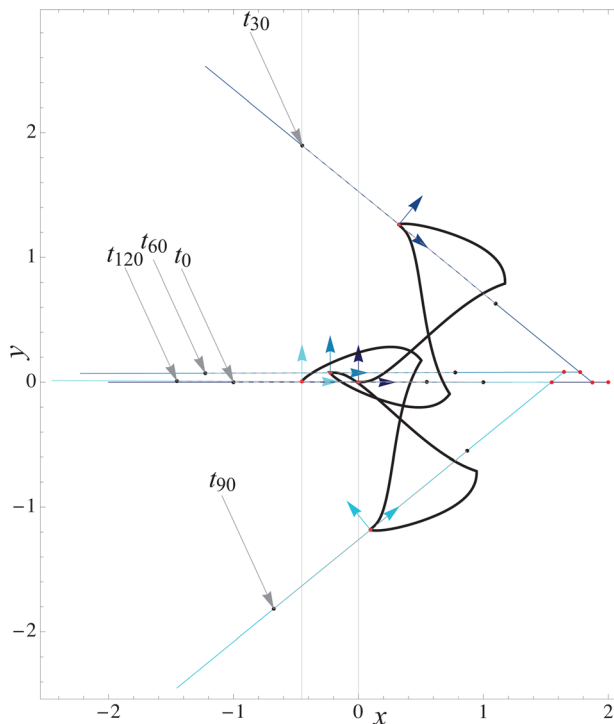


Fig. 10 Net motion along the x direction of the two-link system

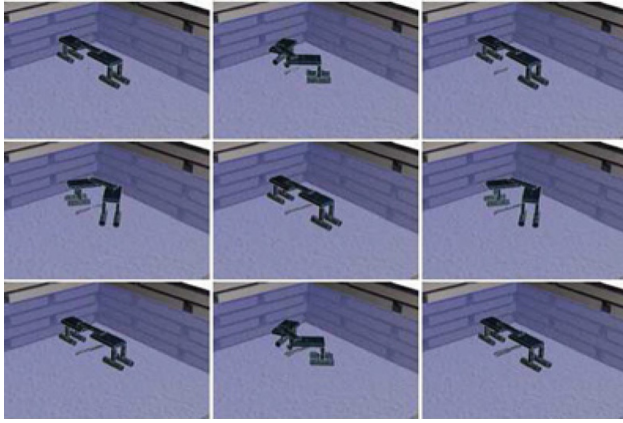


Fig. 11 Simulation using WEBOTS depicting motion along x

we used the same parameter sets given in Eq. (21); however, to model the nonholonomic constraints, we set $\nu = 10000$ and $\mu = 0$.

To compare the locomotion of our proposed system to the roller racer, we simulate the motion of the roller racer for the same input gaits given in Eqs. (27) and (30). Note that, the gait given in Eq. (27), which produced motion along the y direction when implemented on our system, produced *no* net motion when implemented on the roller racer. It can be seen in Fig. 12(a) the body frame of the roller racer (solid lines) returns to its initial location on the inertial origin. In fact, this result is anticipated since the roller racer is a single-input system and thus produces zero “geometric phase-shift” for cyclic motion [36,37]. This is an important property of our proposed system, specifically how drift in the system produced nonzero net motion.

As for the gait given in Eq. (30) that produced a net motion along the x axis, when implemented on the roller racer, a similar behavior is seen in the simulation. The trace of the origin of the body frame and snapshots of its orientation are shown in Fig. 12(b). Note that, the roller racer, as expected produces a larger net motion since it does not have any frictional, i.e., dissipative forces in the system.

5 Discussion and Future Work

The methodology presented in this paper is applicable to systems with more than two links. In fact, the authors have verified the above that the motion planning analysis presented in this paper is adequate for also planar systems with three links. It is important

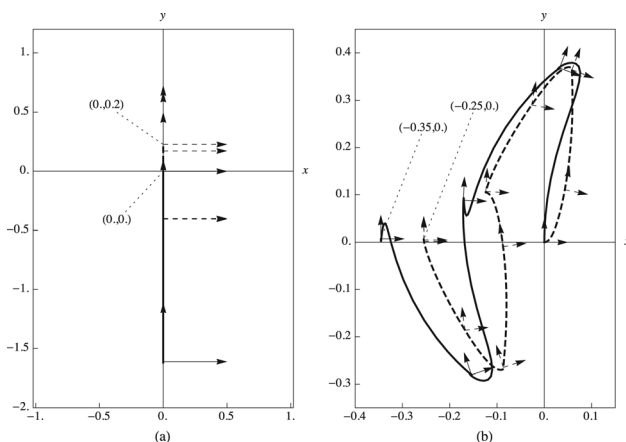


Fig. 12 Motion of the proposed two-link robot in a viscous environment (dashed lines) versus the motion of the roller racer (solid lines). (a) Motion along the y axis. (b) Motion along the x axis.

to note that the gait design exploited both interlink angles rather than locking one of the interlink angles to transform the system into a two-link system. Expanding the results in this paper toward a more general class of mechanical system would be of interest to the authors.

Moreover, another direction, the authors would like to pursue is optimal control. In this paper, we have designed gaits with no regards to any optimality metric. Instead, the gaits were designed to guarantee motion along a desired fiber direction. It would be interesting to introduce an optimality metric into the gait design analysis. This will allow not only for gait that move the system along a desired direction but also do it while minimizing an interesting quantity such as time or control effort.

Another interesting direction of research would be to investigate slow gaits with pulses rather than gaits with active and locked section. The interlink angles will be actuated slowly to render the system kinematic, and then a sudden shape change would be imposed to magnify a certain desired motion.

6 Conclusions

In this paper, we developed a reduced set of the equations of motion for underactuated planar systems. The structure of the equations of motion was investigated and in turn exploited to solve the motion planning problem. In fact, not only we solved for the motion planning problem by specifying the controlled inputs but also by specifying the location of the friction pads in the system. This fact could be used as a design tool to configure robots.

The motion planning analysis was applied on a two-link planar system. Through our analyses, we were able to locomote the system along two desired directions. The gaits were designed to exploit the drift in the system so that a net motion was produced only along the desired direction.

Acknowledgment

This work has been supported by the University Research Board at the American University of Beirut and the Lebanese National Council for Scientific Research. The authors would like to thank the graduate student, Salah Bazzi, for implementing the WEBOTS simulations.

References

- [1] Laumond, J.-P., 1987, “Finding Collision-Free Smooth Trajectories for a Non-Holonomic Mobile Robot,” 10th International Joint Conference on Artificial Intelligence (IJCAI), pp. 1120–1123.
- [2] Laumond, J.-P., Jacobs, P. E., Taix, M., and Murray, R. M., 1994, “A Motion Planner for Nonholonomic Mobile Robots,” *IEEE Trans. Rob. Autom.*, **10**(5), pp. 577–593.
- [3] Li, Z., and Canny, J., 1990, “Motion of Two Rigid Bodies With Rolling Constraint,” *IEEE Trans. Rob. Autom.*, **6**(1), pp. 62–72.
- [4] Laumond, J.-P., 1986, “Feasible Trajectories for Mobile Robots With Kinematic and Environment Constraints,” Intelligent Autonomous Systems, International Conference, North-Holland Publishing Co., Amsterdam, The Netherlands, pp. 346–354.
- [5] Murray, R. M., and Sastry, S. S., 1993, “Nonholonomic Motion Planning: Steering Using Sinusoids,” *IEEE Trans. Autom. Control*, **38**(5), pp. 700–716.
- [6] Barraquand, J., and Latombe, J.-C., 1991, “Robot Motion Planning: A Distributed Representation Approach,” *Int. J. Rob. Res.*, **10**(6), pp. 628–649.
- [7] Canny, J., 1988, *The Complexity of Robot Motion Planning*, MIT Press, Cambridge, MA.
- [8] Lafferriere, G., and Sussmann, H. J., 1993, “A Differential Geometric Approach to Motion Planning,” *Nonholonomic Motion Planning*, Springer, New York, pp. 235–270.
- [9] Bloch, A. M., 2003, *Nonholonomic Mechanics and Control*, Vol. 24, Springer, New York.
- [10] Choset, H. M., 2005, *Principles of Robot Motion: Theory, Algorithms, and Implementation*, MIT Press, Cambridge, MA.
- [11] Bullo, F., 2005, *Geometric Control of Mechanical Systems*, Vol. 49, Springer, New York.
- [12] Tsakiris, D. P., 1995, “Motion Control and Planning for Nonholonomic Kinematic Chains,” DTIC Document, Maryland Univ., College Park Inst. for Systems Research, Technical Report No. ISR-PHD-95-4.
- [13] Krishnaprasad, P., and Tsakiris, D. P., 2001, “Oscillations, SE (2)-Snakes and Motion Control: A Study of the Roller Racer,” *Dyn. Syst.: Int. J.*, **16**(4), pp. 347–397.

- [14] Bloch, A. M., Krishnaprasad, P., Marsden, J. E., and Murray, R. M., 1996, "Nonholonomic Mechanical Systems With Symmetry," *Arch. Ration. Mech. Anal.*, **136**(1), pp. 21–99.
- [15] Lafferriere, G., and Sussmann, H., 1990, "Motion Planning for Controllable Systems Without Drift: A Preliminary Report," Rutgers University Systems and Control Center, Report No. SYCON-90-04.
- [16] Sussmann, H. J., 1991, "Local Controllability and Motion Planning for Some Classes of Systems With Drift," *30th IEEE Conference*, Brighton, Dec. 11–13, pp. 1110–1114.
- [17] Ladd, A. M., and Kavraki, L. E., 2005, "Motion Planning in the Presence of Drift, Underactuation and Discrete System Changes," *Robotics: Science and Systems*, pp. 233–240.
- [18] Mason, R., and Burdick, J., 1999, "Propulsion and Control of Deformable Bodies in an Ideal Fluid," *IEEE International Conference on Robotics and Automation*, Detroit, MI, Vol. 1, pp. 773–780.
- [19] Kanso, E., Marsden, J. E., Rowley, C. W., and Melli-Huber, J., 2005, "Locomotion of Articulated Bodies in a Perfect Fluid," *J. Nonlinear Sci.*, **15**(4), pp. 255–289.
- [20] Kanso, E., and Marsden, J., 2005, "Optimal Motion of an Articulated Body in a Perfect Fluid," 44th IEEE Conference on Decision and Control, 2005 and 2005 European Control Conference (CDC-ECC'05), Dec. 12–15, pp. 2511–2516.
- [21] Melli, J. B., Rowley, C. W., and Rufat, D. S., 2006, "Motion Planning for an Articulated Body in a Perfect Planar Fluid," *SIAM J. Appl. Dyn. Syst.*, **5**(4), pp. 650–669.
- [22] Melsaac, K., and Ostrowski, J., 1999, "A Geometric Approach to Anguilliform Locomotion: Modelling of an Underwater Eel Robot," *IEEE International Conference on Robotics and Automation*, Vol. 4, pp. 2843–2848.
- [23] Chernous'ko, F., 1999, "The Wavelike Motion of a Multilink System on a Horizontal Plane," *J. Appl. Math. Mech.*, **64**(4), pp. 497–508.
- [24] Chernous'ko, F., 2001, "Controllable Motions of a Two-Link Mechanism Along a Horizontal Plane," *J. Appl. Math. Mech.*, **65**(4), pp. 565–577.
- [25] Chernous'ko, F., 2005, "Modelling of Snake-Like Locomotion," *Appl. Math. Comput.*, **164**(2), pp. 415–434.
- [26] Chernous'ko, F., and Shunderyuk, M. M., 2010, "The Influence of Friction Forces on the Dynamics of a Two-Link Mobile Robot," *Appl. Math. Comput.*, **74**, pp. 13–23.
- [27] Figurina, T., 2004, "Quasi-Static Motion of a Two-Link System Along a Horizontal Plane," *Multibody Syst. Dyn.*, **11**(3), pp. 251–272.
- [28] Burton, L. J., Hatton, R. L., Choset, H., and Hosoi, A. E., 2010, "Two Link Swimming Using Buoyant Orientation," *Phys. Fluids*, **22**(9), p. 091703.
- [29] Melli, J., and Rowley, C., 2010, "Models and Control of Fish-Like Locomotion," *Exp. Mech.*, **50**(9), pp. 1355–1360.
- [30] Babikian, S., Shamma, E., and Asmar, D., 2012, "Motion Planning for a Two-Link Planar Robot in a Viscous Environment," *IEEE International Conference on Intelligent Robots and Systems (IROS)*, Vilamoura, Oct. 7–12, pp. 888–895.
- [31] Greenwood, D., 1988, *Principles of Dynamics*, Prentice-Hall, Upper Saddle River, NJ.
- [32] Fiedler, M., 1986, *Special Matrices and Their Applications in Numerical Mathematics*, 1st ed., Springer, New York.
- [33] Bloch, A., Krishnaprasad, P., Marsden, J., and Ratiu, T., 1996, "The Euler-Poincaré Equations and Double Bracket Dissipation," *Commun. Math. Phys.*, **175**(1), pp. 1–42.
- [34] Ostrowski, J., 1998, "Reduced Equations for Nonholonomic Mechanical Systems With Dissipative Forces," *Rep. Math. Phys.*, **42**(1–2), pp. 185–209.
- [35] Murray, R. N., Li, Z., and Sastry, S., 1994, *A Mathematical Introduction to Robotics Manipulation*, CRC Press, Boca Raton, FL.
- [36] Shamma, E. A., 2006, "Generalized Motion Planning for Underactuated Mechanical Systems," Ph.D. thesis, Carnegie Mellon University, Pittsburgh, PA.
- [37] Shamma, E. A., Choset, H., and Rizzi, A. A., 2007, "Towards a Unified Approach to Motion Planning for Dynamic Underactuated Mechanical Systems With Non-Holonomic Constraints," *Int. J. Rob. Res.*, **26**(10), pp. 1075–1124.